

Cl electrosorption on Ag(100): Lateral interactions and electrosorption valency from comparison of Monte Carlo simulations with chronocoulometry experiments

I. Abou Hamad^{1,2}, S.J. Mitchell^{3,4}, Th. Wandlowski⁵, P.A. Rikvold^{1,2}, and G. Brown^{2,6}

¹*Center for Materials Research and Technology and Department of Physics, Florida State University, Tallahassee, FL 32306-4350, USA*

²*School of Computational Science, Florida State University, Tallahassee, FL 32306-4120, USA*

³*Schuit Institute for Catalysis and Department of Chemical Engineering, Eindhoven University of Technology, 5600 MB Eindhoven, The Netherlands*

⁴*The Center for Simulational Physics and The Department of Physics and Astronomy, The University of Georgia, Athens, GA 30602-2451*

⁵*Institute for Thin Films and Interfaces, ISG 3, and Center of Nanoelectronic Systems, cni, Research Centre Jülich, 52425 Jülich, Germany*

⁶*Center for Computational Sciences, Oak Ridge National Laboratory, Oak Ridge, TN 37831, USA*

November 18, 2018

Abstract

We present Monte Carlo Simulations using an equilibrium lattice-gas model for the electrosorption of Cl on Ag(100) single-crystal surfaces. Fitting the simulated isotherms to chronocoulometry experiments, we extract parameters such as the electrosorption valency γ and the next-nearest-neighbor lateral interaction energy ϕ_{nnn} . Both coverage-dependent and coverage independent γ were previously studied, assuming a constant ϕ_{nnn} [I. Abou Hamad, Th. Wandlowski, G. Brown, P.A. Rikvold, *J. Electroanal. Chem.* 554-555 (2003) 211]. Here, a self-consistent, entirely electrostatic picture of the lateral interactions with a coverage-dependent ϕ_{nnn} is developed, and a relationship between ϕ_{nnn} and γ is investigated for Cl on Ag(100).

Keywords: Chlorine electrosorption; Lateral interactions; Electrosorption valency; Chronocoulometry; Continuous phase transition; Lattice-gas model; Monte Carlo simulation.

1 Introduction

Studies of lateral interactions between adsorbed particles are motivated by the need to understand the origin of the wide variety of ordered overlayers and phase transitions at fractional adsorbate coverage on metal surfaces. These interactions have contributions ranging from short-range and van der Waals to long-range dipole-dipole, and lattice-mediated interactions [1]. Hard-square short-range interactions and dipole-dipole long-range interactions are the major contributions to the lateral interactions for bromine adsorption on Ag(100) [2]. In this paper, we explore the validity and applicability of such a model for adsorption of chlorine on Ag(100).

Halide electrosorption on single-crystal metal electrode surfaces is a good model system for studying the properties of the electrode-electrolyte interface in an electrochemical cell. Due to its relative simplicity, it can be used to distinguish between the various contributions of different parameters according to the effect of their inclusion on the overall behavior of the system. A mean-field approach is not sufficient, even for the description of one of the simplest halide-electrosorption systems Br/Ag(100). However, a simple lattice-gas model with constant parameters is sufficient to describe its equilibrium [2, 3], and dynamic [4] properties. While the electrosorption of Br on single-crystal Ag(100) from aqueous solution has been extensively studied as an example of adlayer formation in an electrochemical system [2, 5, 6, 7, 8], less attention has been given to the electrosorption of Cl [3, 9, 10] on Ag(100). A lattice-gas model with constant parameters is not sufficient to describe Cl/Ag(100), therefore this system can be used to further investigate the nature and characteristics of the lateral interactions between the adsorbed halide atoms. In particular, we here develop a self-consistent picture of variable lattice-gas parameters based on the resident charge on the adatoms being coverage dependent or electrode-potential dependent (through the coverage).

The rest of this paper is organized as follows. In Section 2 we describe an electrostatic model of the adlayer that is used in the simulations, the lateral interaction energies, and the Monte Carlo methods used. A brief description of the experimental procedure is given in Section 3. The results of fitting the simulations to experimental data are detailed in Section 4, followed by a brief comparison with Br/Ag(100) in Section 5. Our conclusions are summarized in Section 6.

2 Self-consistent electrostatic adlayer model

2.1 Lattice-gas model

The adsorption of Cl ions occurs at the fourfold hollow sites of the Ag(100) surface [11], which form a square lattice as shown in Fig. 1. To approximate the equilibrium behavior of this system, we use a lattice-gas model, in which the lattice sites correspond to the adsorption sites. Mitchell *et al.* [12] used an off-lattice model for the Br/Ag(100) system to show that the Br adsorbates spend most of the time near the four-fold hollow sites of the Ag(100) surface, thus justifying the lattice-gas treatment of halide adsorption. To describe the energy associated with a configuration of adsorbates on the surface, a grand-canonical effective Hamiltonian [2, 6, 13, 14] is used,

$$\mathcal{H} = - \sum_{i < j} \phi_{ij} c_i c_j - \bar{\mu} \sum_{i=1}^N c_i , \quad (1)$$

where $\sum_{i < j}$ is a sum over all pairs of sites, ϕ_{ij} are the lateral interaction energies between particles on the i th and j th lattice sites, measured in meV/pair, $\bar{\mu}$ is the electrochemical potential, measured in meV/particle, and $N = L^2$ is the total number of lattice sites. The local occupation variable c_i is 1 if site i is occupied and 0 otherwise.

The long-range interactions, ϕ_{ij} , depend on the distance, r_{ij} , between ions i and j (measured in Ag(100) lattice spacing units, $a = 2.889 \text{ \AA}$ [7]) as

$$\phi_{ij} = \begin{cases} -\infty & r_{ij} = 1 \\ \frac{2^{3/2} \phi_{\text{nnn}}}{r_{ij}^3} & r_{ij} \geq \sqrt{2} \end{cases} , \quad (2)$$

where the infinite value for $r_{ij} = 1$ indicates nearest-neighbor exclusion, and negative values of ϕ_{ij} denote long-range repulsion. The coverage isotherms were simulated using a square $L \times L$ lattice with periodic boundary conditions to reduce finite-size effects.

The electrochemical potential $\bar{\mu}$ is related to the bulk ionic concentration C and the electrode potential E (measured in mV). In the dilute-solution approximation, the relationship is

$$\bar{\mu} = \bar{\mu}_0 + k_B T \ln \left(\frac{C}{C_0} \right) - e \int_{E_0}^E \gamma(E') dE' , \quad (3)$$

where $\bar{\mu}_0$ is an arbitrary constant, C_0 is a reference concentration (here taken to be 1 mM), and e is the elementary charge unit [15]. The reference potential E_0 is chosen sufficiently negative such that the coverage vanishes at E_0 for all values of C used, and $\bar{\mu}$ has the sign convention that $\bar{\mu} > 0$ favors adsorption. The relationship between $\bar{\mu}$, C , and E is discussed further in the Appendix.

2.2 Lateral interaction energies

When Cl ions adsorb on the surface, a fraction of their charge is transferred through the external circuit. This fraction, γe , is negative and is directly related to the average resident charge per ion, $q = -(1 + \gamma)e$ [16]. This relationship is an approximation and is more valid as the potential at the adsorbate approaches the value of the potential in the solution. For the current system's ionic strength, this condition is only approximately satisfied and may be considered as a source of error.

We have previously shown [3] that for Cl/Ag(100), the electrosorption valency γ depends on the coverage θ , which is defined as

$$\theta = N^{-1} \sum_{i=1}^N c_i . \quad (4)$$

In order to investigate such a dependence more thoroughly, we here propose a model with a coverage-dependent next-nearest-neighbor lateral interaction energy ϕ_{nnn} , as well. This is motivated by two assumptions: that γ is coverage dependent and that the major contribution to ϕ_{nnn} is due to electrostatic dipole-dipole interactions. A simple electrostatic picture of the adlayer, in which an adsorbate's resident charge and its image charge form a dipole, suggests a relationship between the electrosorption valency and the dipole moment. If γ is coverage dependent ($\gamma = \gamma(\theta)$), then the resident charge is also coverage dependent ($q = q(\theta)$), and hence ϕ_{nnn} , which is proportional to q^2 , is coverage dependent as well ($\phi_{\text{nnn}} = \phi_{\text{nnn}}(\theta)$).

Assuming for simplicity that γ depends linearly on θ ,

$$\gamma = \gamma_0 + \gamma_1 \theta , \quad (5)$$

the resident charge q becomes

$$q = -(1 + \gamma_0 + \gamma_1 \theta)e , \quad (6)$$

and ϕ_{nmn} takes the form:

$$\phi_{\text{nmn}} = A(1 + \gamma_0 + \gamma_1\theta)^2, \quad (7)$$

where A is a prefactor proportional to the square of a “dipole distance”. This effect is known as *depolarization*, and may under extreme conditions lead to the possibility of a first-order phase transition [17, 18]¹. If γ is coverage independent (i.e., $\gamma_1 = 0$), then ϕ_{nmn} becomes coverage independent, as well.

2.3 Monte Carlo method

Equilibrium Monte Carlo (MC) simulations were used to measure the equilibrium coverage as a function of $\bar{\mu}$, which was then converted to E using Eq. (3). At each MC step a lattice site, i , was chosen randomly, and a change in its occupation variable c_i was attempted with a Metropolis acceptance probability [19]:

$$\mathcal{R} = \min \left[1, \exp \left(-\frac{\Delta\mathcal{H}}{k_{\text{B}}T} \right) \right], \quad (8)$$

where $\Delta\mathcal{H}$ is the energy difference between the initial state and the proposed state. The value of ϕ_{nmn} was updated in the simulations at each MC step, corresponding to the new proposed coverage.

The energy difference $\Delta\mathcal{H}$ was calculated from Eq. (1) using two methods, a truncated sum of the contributions of neighboring occupied sites up to five lattice spacings away [2, 3, 6], and a mean-field-enhanced truncated sum up to three lattice spacings [3]. In the latter method, energy contributions from adparticles more than three lattice spacings away are calculated using a mean-field estimate as detailed in Ref. [3].

3 Experimental

A detailed description of the experimental procedure is given in Ref. [3, 8], and only a brief summary follows here. The Ag(100) single-crystal electrodes were chemically etched in cyanide solution, rinsed in Milli-Q water, and carefully annealed in a hydrogen flame. They were then quickly transferred into

¹For our model of Cl adsorption on Ag(100) with the fitting parameters obtained in this paper, the first-order phase transition is not observed in the simulations, even for temperatures as unrealistically low as 1 K. The model does produce a first-order transition at room temperature for some parameters that do not fit the experimental data.

the electrochemical cell after cooling in a stream of Argon. Using the hanging meniscus technique, a platinum wire counter electrode, and a saturated calomel electrode as reference electrode, the electrochemical measurements were carried out at a temperature of $(20 \pm 1)^\circ\text{C}$.

For the chronocoulometric experiments, the potential was set at initial values between -1.375 and -0.300 V vs SCE until adsorption equilibrium was established, and then stepped to the final potential of -1.400 V, where the chloride is completely desorbed from the surface.

4 Results

The equilibrium MC simulations were performed at a temperature of 17°C for various values of A , γ_0 , and γ_1 . The value of A was varied from 0 to -100 meV in steps of 5 meV, while γ_0 and γ_1 were varied from 0 to -0.9 in steps of 0.1, resulting in 2000 different simulations. The resulting simulated isotherms were fitted to experimental data. This large number of simulations necessitated the choice of the relatively small system size with $L = 32$. The system displays a second-order phase transition from a disordered, low-density phase to an ordered $c(2 \times 2)$ phase [2] at an intermediate value of the electrochemical potential. For the steepest part of the isotherm (Fig. 2), where critical slowing down due to the phase transition is important, the system was allowed to relax for a longer time to reach equilibrium than for the points further away from the phase transition. We checked for finite-size effects, and no significant difference was observed when comparing the resulting isotherms with isotherms simulated using larger system sizes of $L = 64, 128$, and 256 . A small value of L can be used because θ is not the order parameter corresponding to the $c(2 \times 2)$ phase, and so its fluctuations, which are proportional to $d\theta/d\bar{\mu}$, only diverge logarithmically with L [2, 20, 21]. In addition, better statistics were collected close to the phase transition, using longer runs and more sampling than for points far from the phase transition, where the fluctuations are smaller.

Using Eq. (3), the simulated isotherms were converted from the $\bar{\mu}$ scale to the E scale and then fit to the experimental isotherms. The fitting was done by varying the value of $\bar{\mu}_0$ to minimize $\hat{\chi}^2$ for each set of values for A ,

γ_0 , and γ_1 . Here,

$$\hat{\chi}^2 = \frac{\sum_{\text{exp points}} (\theta_{\text{exp}} - \theta_{\text{sim}})^2}{\text{degrees of freedom}} \quad (9)$$

is the least-squares sum per degree of freedom, and θ_{exp} and θ_{sim} are the experimental and simulated coverages, respectively, corresponding to the same value of E . Linear interpolation was used between the simulated data points to calculate θ_{sim} for all values of E .

From fits to 10 mM and 20 mM experiments, a grid of values of $\hat{\chi}^2$, was collected. Three different models were studied. (i) A constant γ (i.e., also constant ϕ_{nnn}) model for which we only considered the simulations with $\gamma_1 = 0$. (ii) A model in which only the line with $\gamma_0 = -0.3$, $\gamma_1 = -0.3$ was considered. These values for γ_0 and γ_1 were estimated from values of γ obtained from the experimental data in Ref. [3] using the method in Ref. [22]. (iii) The third model studied was the coverage dependent model with $\phi_{\text{nnn}} = \phi_{\text{nnn}}(\gamma(\theta))$, where no constraints on the values of any of the parameters were imposed, and the whole parameter space was searched for a global minimum.

A three-dimensional plot of the parameter space is shown in Fig. 3(a), where the diameters of the symbols are proportional to $1/\hat{\chi}^2$ for fits to 20 mM (circles) and 10 mM (squares) of the mean-field-enhanced simulations. The parameter space for the non-mean-field-enhanced method (not shown) is similar. Figure 3(a) shows the existence of several local minima and a good overlap between the minima for both concentrations. The position of the accepted global minimum is indicated by the arrows. Figure 3(b) is a projection onto the γ_0, γ_1 plane, which shows that the minima are concentrated within one region close to the $\gamma_1 = 0$ plane, suggesting a relatively weak dependence of γ on the coverage. Moreover, the $\hat{\chi}^2$ values in the $\gamma_1 = 0$ plane (model (i)) and for $\gamma_0 = \gamma_1 = -0.3$ (model (ii)) are significantly larger than the $\hat{\chi}^2$ values for the accepted global minimum (model (iii)). Figures 3(c) and 3(d) show that while the magnitude of γ_0 decreases monotonically with increasing A , there is no general trend for γ_1 as a function of A .

Due to the existence of several shallow minima of $\hat{\chi}^2$, and due to the limited resolution of the grid in parameter space, we list in Table 1 the best-fit parameter values for each model, along with all fits that have $\hat{\chi}^2$ within 10% of the best-fit value. One can see in Table 1 that there are two possible sets of parameters that fit to the 10 mM data for model (iii) with mean-field-enhanced simulations. To discriminate between these possible fits to the 10 mM data we check if they are also possible fits to the 20 mM experimental

data. The first set ($A = -90$ meV) is the overall best fit for 10 mM. However, it fits only slightly better than the second set ($A = -55$ meV), and it is not a possible fit to the 20 mM experimental data. The only parameter set ($A = -55$ meV, $\gamma_0 = -0.4$, $\gamma_1 = -0.2$) that is a possible fit to both the 10 mM and 20 mM experimental data, is the accepted best fit for model (iii). Using the same approach for the non-mean-field-enhanced method, models (i) and (ii), and concentration, results in a unique set of parameter values for each model, simulation method, and concentration. These accepted fits are summarized in Table 2. Notice in Table 2 that for the accepted global minimum of model (iii), and for both mean-field-enhanced and non-mean-field-enhanced methods, the values of γ_0 and γ_1 are reasonably close to the ones calculated from the experimental data [3] using the method of Ref. [22]. Also note that the fits for 10 mM are consistently better than the fits to the 20 mM experiments. This might be due to violation of the dilute-solution limit at the higher concentration. This may also be the reason that the values of $\bar{\mu}_0$, which are expected to be the same for both concentrations when fit to a single simulation, differ consistently by about 12 ± 7 meV between the concentrations. The values of A are consistently less negative for the longer-ranged lateral interactions of the mean-field-enhanced than for the non-mean-field method. This is not surprising.

The quality of the fits is better for model (iii), as can be seen from the plots corresponding to each of the models (Figs. 2, 4, and 5). Models (ii) and (i) fit worse at either the lower-coverage part of the isotherm (model (ii)), see Fig. 4, or at the upper part of the isotherm (model (i)), see Fig. 5. In contrast, the best-fit simulations in Fig. 2 fit the experiments well over the whole range of coverages. The plots for the non-mean-field-enhanced fits (not shown) are similar. A plot of γ vs E is shown in Fig. 6(a) for the best-fit values of γ_0 and γ_1 corresponding to the 10 mM experimental data for each of the three models considered. Also shown are the values of γ obtained in Ref. [3] by the method of Ref. [22]. While model (ii) is expected to fit the Ref. [3, 22] values of γ , model (iii) also predicts a mean value of γ close to, but slightly more negative than, the mean of the values of γ from Ref. [3, 22]. The ϕ_{nmn} values corresponding to the best fits of the three models are shown in Fig. 6(b).

Since the fits are sometimes better for the mean-field-enhanced method, and sometimes worse, the mean of the sets of parameters obtained by including and excluding the mean-field enhancement are reported here as our final results: $A = -60$ meV, $\gamma_0 = -0.4$, $\gamma_1 = -0.2$, and $\bar{\mu}_0 = -325$ meV. In the

far-field approximation used here, the lateral interaction energy between two parallel dipoles separated by a distance $a\sqrt{2}$ is given by

$$\phi_{\text{nmn}} = \frac{1}{4\pi\epsilon_0} \frac{p^2}{(a\sqrt{2})^3} = A(1 + \gamma_0 + \gamma_1\theta)^2 = A \left(\frac{q}{e}\right)^2, \quad (10)$$

where $p = |q|d$ is the dipole moment, d is an effective “dipolar distance,” and the second and third equalities result from Eqs. (7) and (6), respectively. Consequently,

$$p = \left(\frac{|q|}{e}\right) \sqrt{4\pi\epsilon_0(a\sqrt{2})^3 A}. \quad (11)$$

For the $A = -60$ meV final result, the dipole moment ranges between $p = 0.32$ eÅ for $\theta = 0$ and $p = 0.26$ eÅ for $\theta = 0.5$, and the “dipolar distance” $d \approx 0.53$ Å. Density Functional Theory calculations of a model without water [23] suggest a dipole moment of 0.46 eÅ, which is only about 40% higher than the fitted value at low coverage. From naïve physical intuition, the dipolar distance might be expected to be of the order of the ionic diameter of Cl, about 3Å. The value of d obtained here involves several assumptions. One main assumption used is that the dipole is a classical point dipole, which should be quite reasonable as the distance between neighboring dipoles is about an order of magnitude larger than the obtained value for d . Moreover, we have assumed that the interaction is a classical electrostatic dipole interaction, while there could be quantum effects at the shortest length scales. On the other hand, when viewed as a charge distribution, the dipole is expected to have a much smaller “dipolar distance” than naïvely expected [24]. Using the relationship between the dipole moment and the Helmholtz capacitance C_{H} [16],

$$p = |q|d = \frac{e\epsilon_0}{C_{\text{H}}}(1 + \gamma), \quad (12)$$

and our values for the dipole moment and γ , we obtain a C_{H} that is in the range of 26 to 32 $\mu\text{F}/\text{cm}^2$. This range is comparable to the reported value of C_{H} for Ag(110) in chloride ion solution, $C_{\text{H}} \approx 100$ $\mu\text{F}/\text{cm}^2$ [24], which would yield $d = \epsilon_0/C_{\text{H}} \approx 0.1$ Å. This value of d is of the same order of magnitude as our value.

Finally, although models (i) and (ii) are still possible, a self-consistent ($\phi_{\text{nmn}}(\gamma(\theta))$) entirely electrostatic model not only fits better to the experimental data but also, with no constraints imposed, predicts values of γ that

are reasonably compatible with those obtained from the experimental data using the method of Ref. [22].

5 Comparison to Br/Ag(100)

Br electrosorption on the same substrate Ag(100) displays different characteristics. The electrosorption valency and the next-nearest-neighbor lateral interaction energy are not only more negative, $\gamma = -0.71 \pm 0.01$ and $\phi_{\text{nnn}} = -21 \pm 2$ meV, but also independent of the coverage [3]. In other words, while mutual depolarization [18] is present for Cl/Ag(100), this effect is not significant for Br/Ag(100). Simulations of Br/Ag(100) using $\gamma = \gamma_0 + \gamma_1\theta$, when fit to three experimental data sets, yielded $\gamma_1 \approx 0$ [3]. Moreover, the value obtained for γ (-0.71), is consistent with previous results from both simulations and experimental analysis [2]. Since Cl is more electronegative than Br, it is expected to have a less negative γ or a more negative resident charge, consistent with our results.

6 Conclusion

A discrepancy between the values of the electrosorption valency γ obtained from fitting simulations to experiments, and the value obtained from the analysis [22] of experimental data was reported in a previous study by Abou Hamad *et al.* [3]. This discrepancy suggested that the long-range interactions are dominated by electrostatic dipole/dipole effects for Cl electrosorption on the Ag(100) single crystal surface.

In this work, a large set of MC simulations (2000 simulations) over a grid in parameter space was fitted to two sets of chronocoulometry experimental data for different concentrations. The existence of local minima of $\hat{\chi}^2$ in parameter space suggests alternative models. To within the resolution of our grid and the accuracy of the experimental data, we have shown that while other, simpler, models are still possible, a purely electrostatic model can be used to describe the Cl/Ag(100) system. It also predicts an electrosorption valency that is compatible with the value obtained through direct experimental data analysis by the method of Ref. [22]. Additional sets of experimental data, with different concentrations around 10 and 20 mM of the adsorbate ion, along with a finer grid in parameter space would enable a more decisive

determination of the most appropriate model and its parameter values.

Acknowledgments

We thank M.T.M. Koper and S. Frank for useful discussions and helpful comments. We also thank M.T.M. Koper for bringing Refs. [17, 18] to our attention. This work was supported in part by NSF grant No. DMR-0240078, and by Florida State University through the School of Computational Science and the Center for Materials Research and Technology, the Research Centre Jülich, and the Netherlands Organization for Scientific Research (NWO).

Appendix

In this appendix we discuss the relationship between the electrochemical potential $\bar{\mu}$ and the electrode potential E for a coverage or field dependent electrosorption valency γ .

We define the electrosorption valency as [16]

$$\gamma = - \left(\frac{\partial \sigma_M}{\partial \theta} \right)_E, \quad (13)$$

where σ_M is the charge on the metal, θ is the coverage, and μ is the *chemical* potential of the solution (here taken as the dilute-solution approximation, $\mu = k_B T \ln(\frac{C}{C_0})$). Considering an auxiliary thermodynamic potential X related to the surface tension α as

$$X = \alpha + \theta \mu, \quad (14)$$

and using the Lippman equation,

$$dX = \mu d\theta - \sigma_M dE, \quad (15)$$

we have

$$\left(\frac{\partial X}{\partial E} \right)_\theta = -\sigma_M \text{ and } \left(\frac{\partial X}{\partial \theta} \right)_{\sigma_M} = \mu. \quad (16)$$

Consequently, one obtains the Maxwell relation, [16]

$$\gamma = - \left(\frac{\partial \sigma_M}{\partial \theta} \right)_E = \frac{\partial X}{\partial E \partial \theta} = \left(\frac{\partial \mu}{\partial E} \right)_\theta. \quad (17)$$

The relation, $\gamma = \left(\frac{\partial\mu}{\partial E}\right)_\theta$, gives the electrosorption valency as the change in μ necessary to keep θ constant under a change in E . But to keep θ constant, the *electrochemical* potential $\bar{\mu}$ must remain constant, so that

$$\gamma = \left(\frac{\partial\mu}{\partial E}\right)_\theta \equiv \left(\frac{\partial\mu}{\partial E}\right)_{\bar{\mu}}. \quad (18)$$

It is easy to show that Eq. (3) satisfies this requirement for γ . If

$$\bar{\mu} = \bar{\mu}_0 + k_B T \ln \left(\frac{C}{C_0}\right) - e \int_{E_0}^E \gamma(E') dE',$$

then

$$\mu = \bar{\mu} + e \int_{E_0}^E \gamma(E') dE' + \text{const.}, \quad (19)$$

and

$$\left(\frac{\partial\mu}{\partial E}\right)_\theta = \left(\frac{\partial\mu}{\partial E}\right)_{\bar{\mu}} = \gamma(E). \quad (20)$$

Generalization to multiple adsorbates is straightforward.

References

- [1] T.L. Einstein, in: W.N. Unertl (Ed.), Handbook of Surface Science, vol. 1, Elsevier Science B.V., Amsterdam, 1996, p. 577-650.
- [2] S.J. Mitchell, G. Brown, P.A. Rikvold, Surf. Sci. 471 (2001) 125.
- [3] I. Abou Hamad, Th. Wandlowski, G. Brown, P.A. Rikvold, J. Electroanal. Chem. 554-555 (2003) 211.
- [4] I. Abou Hamad, P.A. Rikvold, G. Brown, Surf. Sci. 572 (2004) L355.
- [5] O. Endo, M. Kiguchi, T. Yokoyama, M. Ito, and T. Ohta. J. Electroanal. Chem., 473 (1999) 19.
- [6] S.J. Mitchell, G. Brown, P.A. Rikvold, J. Electroanal. Chem. 493 (2000) 68.
- [7] B.M. Ocko, J.X. Wang, Th. Wandlowski, Phys. Rev. Lett. 79 (1997) 1511.

- [8] Th. Wandlowski, J.X. Wang, B.M. Ocko, *J. Electroanal. Chem.* 500 (2001) 418.
- [9] O.M. Magnussen, *Chem. Rev.* 102 (2002) 679.
- [10] G. Valette, A. Hamelin, R. Parsons, *Z. Phys. Chem. Neue Fol.* 113 (1978) 71.
- [11] Th. Wandlowski, B.M. Ocko, J.X. Wang, in preparation (2005).
- [12] S.J. Mitchell, S.W. Wang, P.A. Rikvold, *Faraday Disc.* 121 (2002) 53.
- [13] M.T.M. Koper, *J. Electroanal. Chem.* 450 (1998) 189.
- [14] M.T.M. Koper, *Electrochim. Acta* 44 (1998) 1207.
- [15] K.J. Vetter, J.W. Schultze, *Ber. Bunsenges. Phys. Chem.* 76 (1972) 920; *ibid* 76 (1972) 927.
- [16] W. Schmickler, *Interfacial Electrochemistry*, Oxford Univ. Press, New York Oxford, 1996, Chapter 18.
- [17] L.D. Roelofs, D.B. Fromowitz, *Surf. Sci.* 388 (1997) 92.
- [18] M.T.M. Koper, *Surf. Sci.* 395 (1998) L196.
- [19] D.P. Landau, K. Binder, *A Guide to Monte Carlo Simulations in Statistical Physics*, Cambridge Univ. Press, Cambridge, 2000.
- [20] K. Binder, *Ann. Rev. Phys. Chem.* 43 (1992) 33.
- [21] P.A. Rikvold, *Phys. Rev. B* 32 (1985) 4756; Erratum: *Phys. Rev. B* 33 (1986) 6523.
- [22] J. Lipkowski, J. Stolberg, in: J. Lipkowski, P.N. Ross, (Eds.), *Adsorption of Molecules at Metal Electrodes*, VCH Publishers, New York, 1992, pp. 171-238.
- [23] I. Abou Hamad, S.J. Mitchell, M.T.M. Koper, unpublished.
- [24] W. Schmickler, *J. Electroanal. Chem.* 249 (1988) 25.

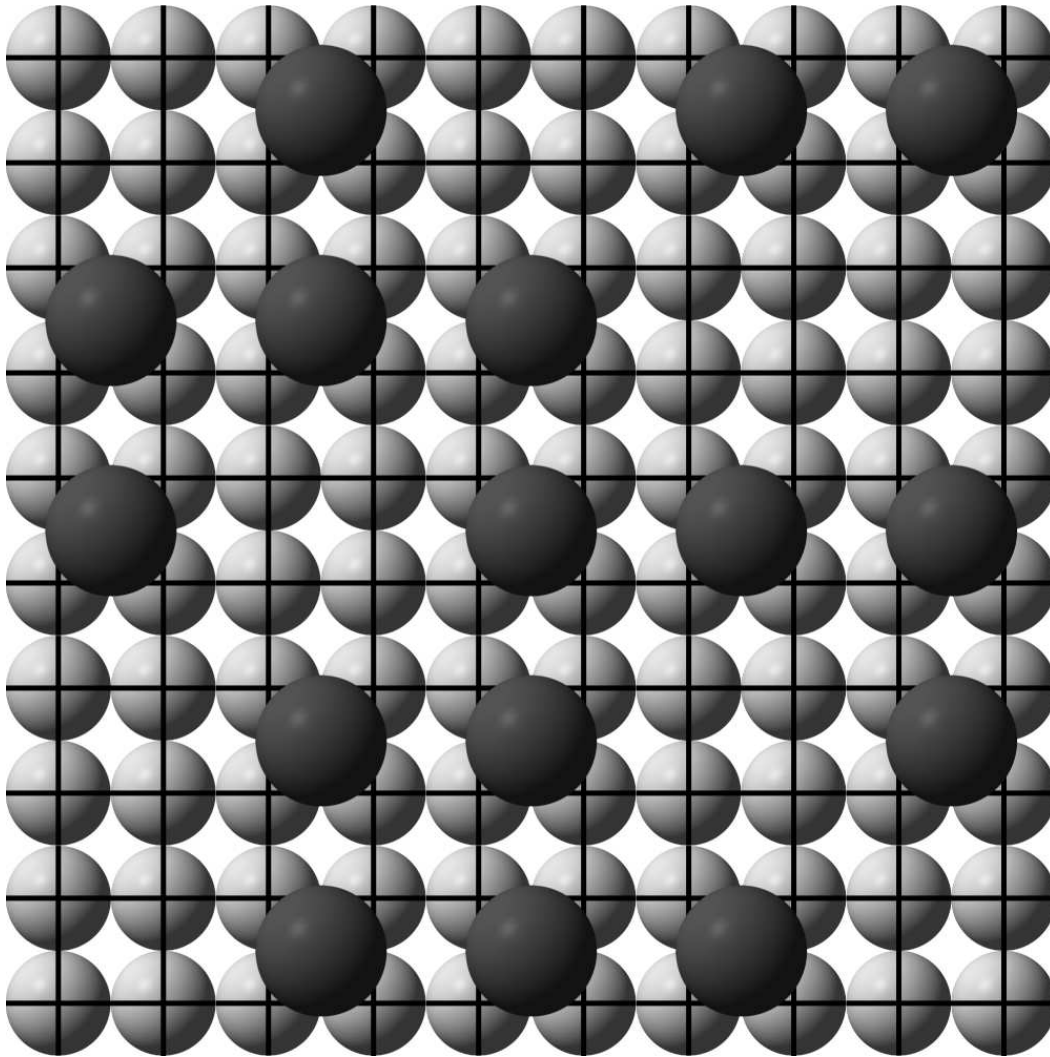


Figure 1: Cl (larger, dark gray, spheres) adsorbed at the 4-fold hollow sites of the (100) surface of Ag (smaller, lighter gray, spheres). The grid frame corresponds to the lattice of adsorption sites. The figure is drawn approximately to scale.

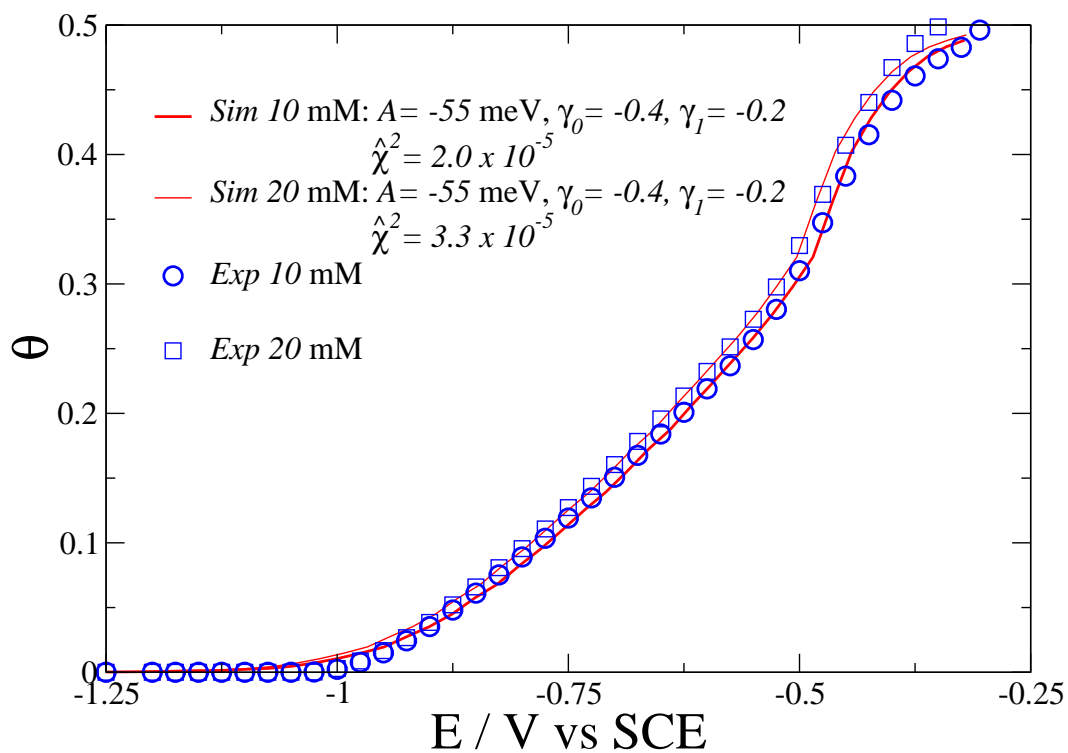


Figure 2: Best fit of mean-field-enhanced simulation to experimental 10 mM and 20 mM coverage isotherms: $A = -55 \text{ meV}$, $\gamma_0 = -0.4$, and $\gamma_1 = -0.2$ (model (iii)). $L = 32$.

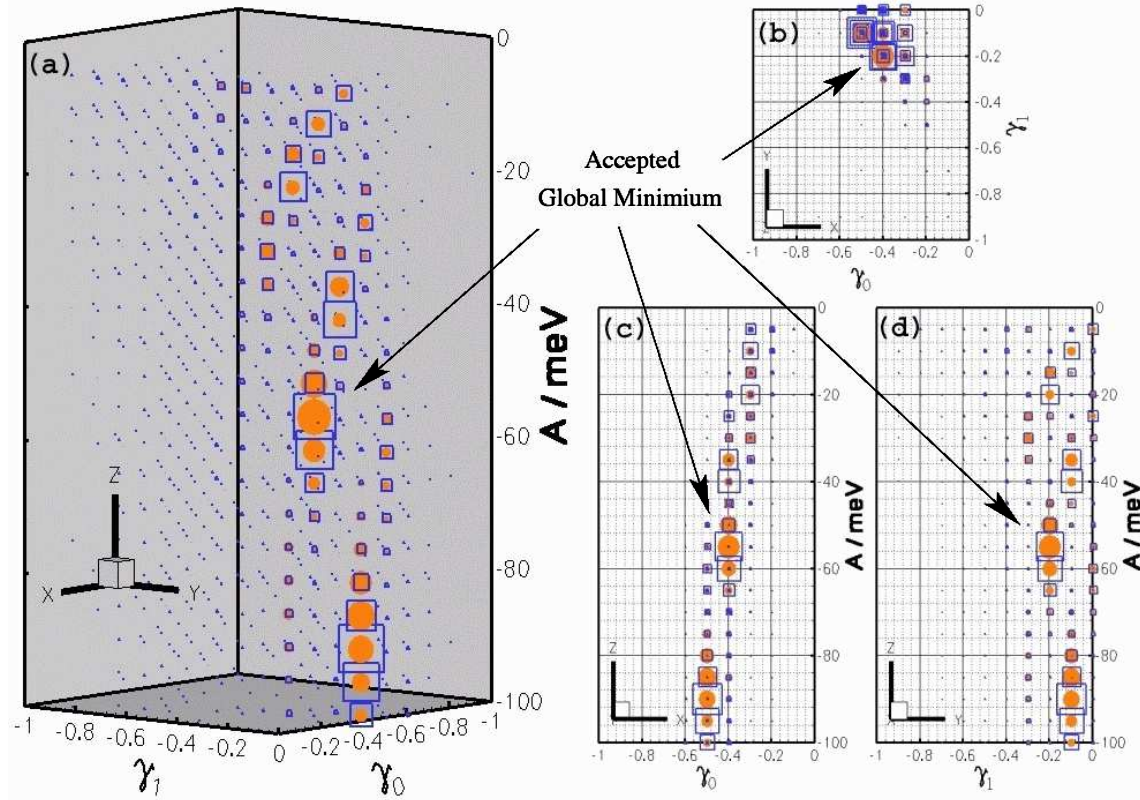


Figure 3: A plot of $1/\chi^2$ in the three-dimensional parameter space, obtained from fits of mean-field-enhanced simulations to the 10 mM experimental data (squares) and the 20 mM experimental data (circles). The diameters of the symbols are proportional to $1/\chi^2$. (a) is a three dimensional view, (b) is a projection onto the γ_0 , γ_1 plane, and (c) and (d) are projections onto the γ_0 , A plane and the γ_1 , A , plane respectively. The parameter space for the non-mean-field-enhanced method (not shown) is similar.

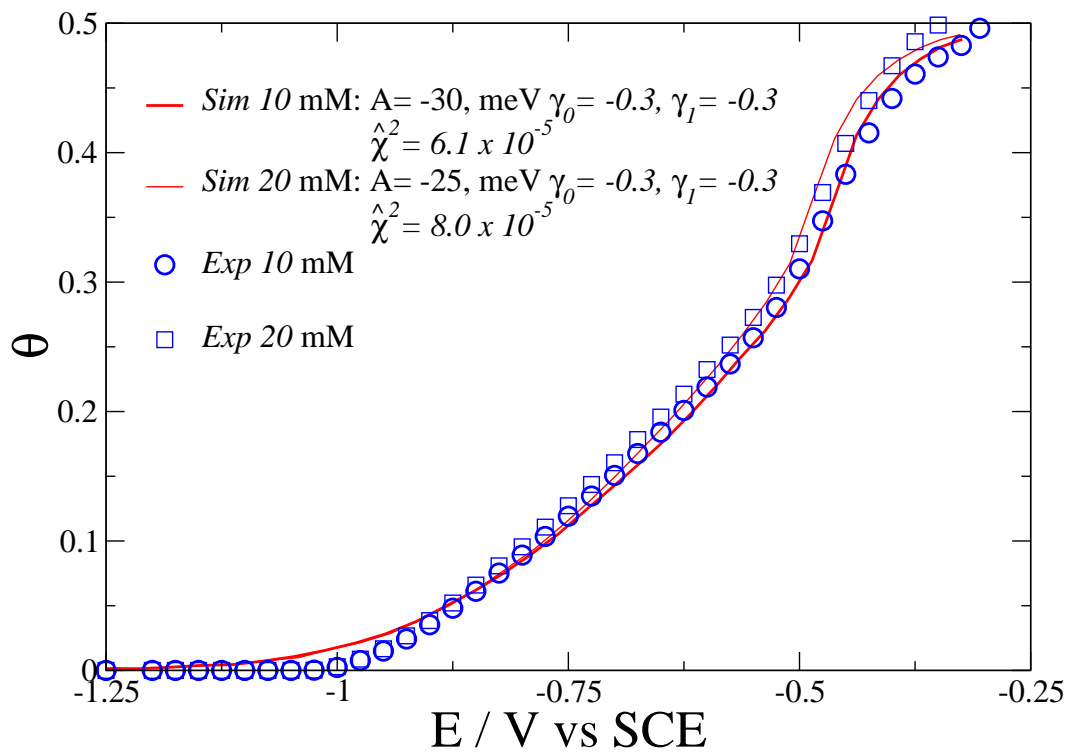


Figure 4: Simulated constrained best fit with the values of $\gamma_0 = -0.3$ and $\gamma_1 = -0.3$ (model (ii)) for the 10 and 20 mM experimental data. Mean-field-enhanced simulations are shown here. $L = 32$.

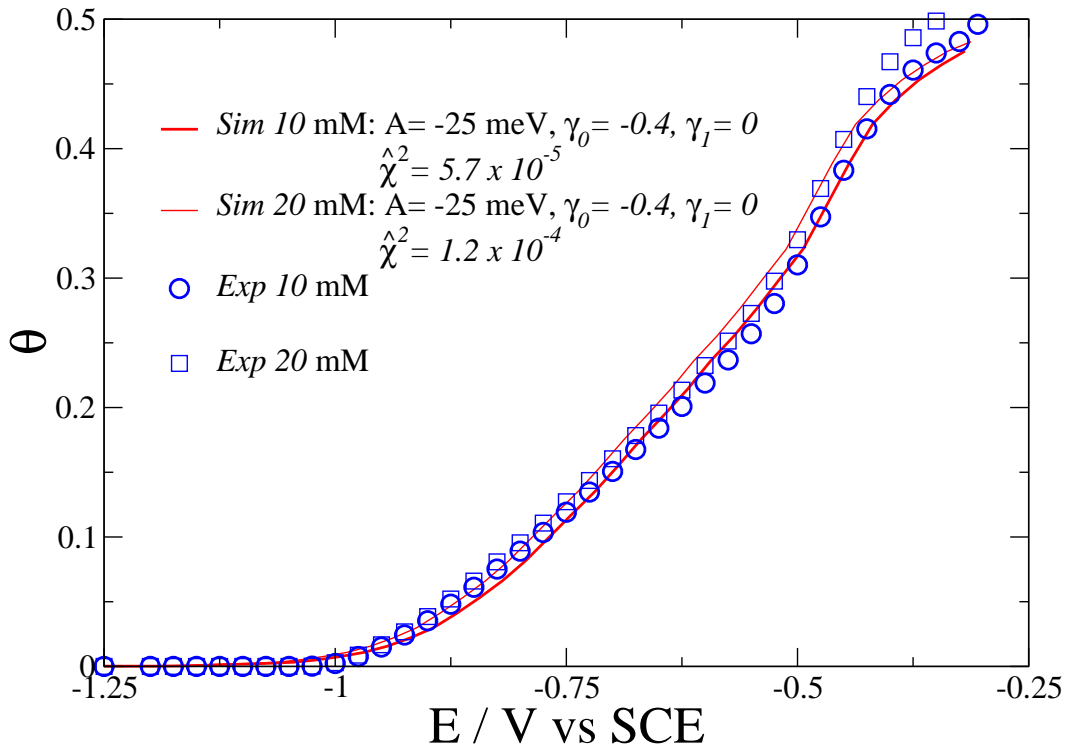


Figure 5: Simulated constrained best fit with a constant γ (model (i)) for the 10 and 20 mM experimental data. Mean-field-enhanced simulations are shown here. $L = 32$.

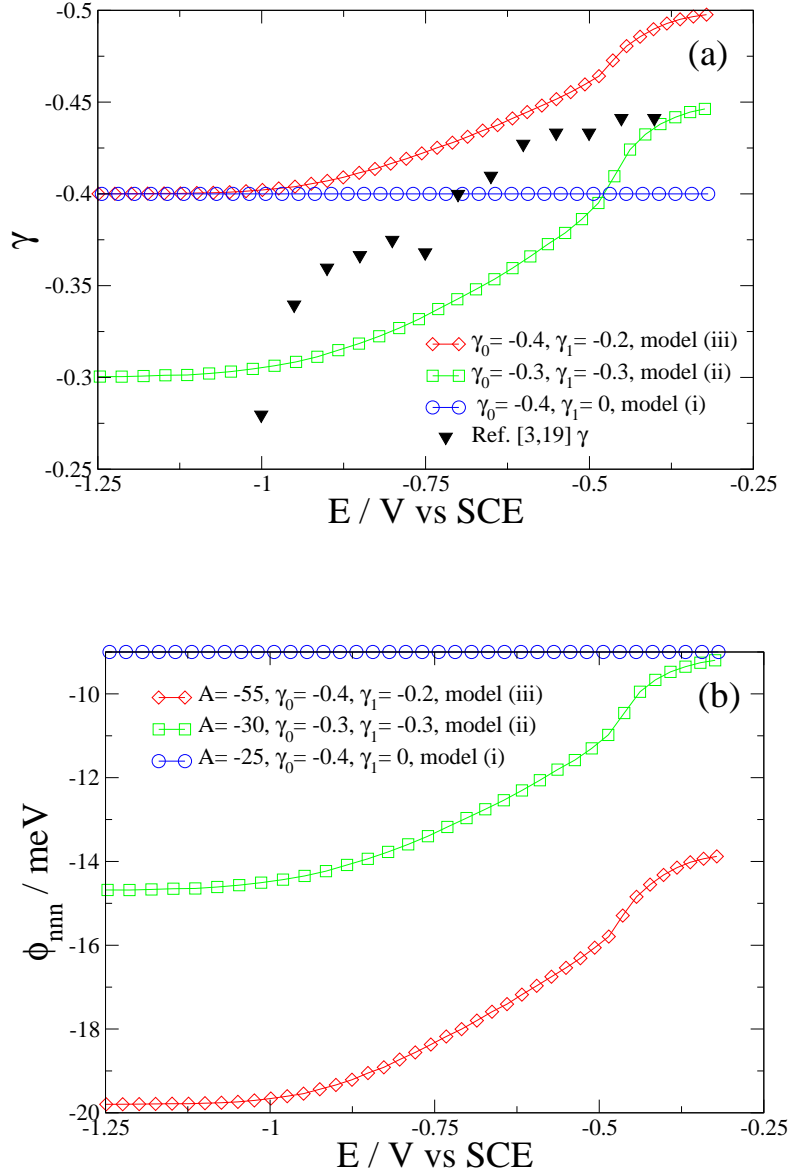


Figure 6: (a) The electroadsorption valency γ vs E for the values of γ_0 and γ_1 obtained from the best fits for models (i), (ii), and (iii) to the 10 mM experimental data. The values of γ obtained in Ref. [3] by the method of Ref. [22] are also shown. (b) Corresponding plots of ϕ_{nnn} vs E for the three models.

Table 1: Fitting parameters for Cl adsorption on a Ag(100) single-crystal surface, for models (i), (ii), and (iii), with and without mean-field interactions. Possible fits to within 10% of the best $\hat{\chi}^2$ for each model are also shown. A and $\bar{\mu}_0$ are in units of meV.

Model	Mean-field enhanced									
	10 mM					20 mM				
	A	γ_0	γ_1	$\bar{\mu}_0$	$\hat{\chi}^2 \times 10^5$	A	γ_0	γ_1	$\bar{\mu}_0$	$\hat{\chi}^2 \times 10^5$
(i) Const. γ	-25	-0.4	0	-330	5.664	-60	-0.5	0	-390	11.927
	-5	-0.3	0	-281	5.769	-55	-0.5	0	-396	11.942
						-25	-0.4	0	-340	12.079
						-20	-0.4	0	-349	12.514
(ii) Ref. [3, 22] γ	-30	-0.3	-0.3	-266	6.068	-25	-0.3	-0.3	-285	8.037
(iii) $\phi_{\text{mnn}}(\gamma(\theta))$	-90	-0.5	-0.1	-371	1.815	-55	-0.4	-0.2	-328	3.340
	-55	-0.4	-0.2	-318	1.976					
(i) Const. γ	No mean-field enhancement									
		A	γ_0	γ_1	$\bar{\mu}_0$	$\hat{\chi}^2 \times 10^5$	A	γ_0	γ_1	$\bar{\mu}_0$
(i) Const. γ	-30	-0.4	0	-330	5.369	-70	-0.5	0	-393	11.246
						-30	-0.4	0	-341	11.330
						-65	-0.5	0	-398	11.350
						-25	-0.4	0	-348	11.606
(ii) Ref. [3, 22] γ	-35	-0.3	-0.3	-268	6.086	-30	-0.3	-0.3	-286	7.462
(iii) $\phi_{\text{mnn}}(\gamma(\theta))$	-45	-0.4	-0.1	-325	2.310	-65	-0.4	-0.2	-330	3.112
	-65	-0.4	-0.2	-320	2.311					

Table 2: The best-fit parameters for Cl adsorption on a Ag(100) single-crystal surface, for models (i), (ii), and (iii), with and without mean-field interactions. A and $\bar{\mu}_0$ are in units of meV.

Model	Mean-field enhanced									
	10 mM					20 mM				
	A	γ_0	γ_1	$\bar{\mu}_0$	$\hat{\chi}^2 \times 10^5$	A	γ_0	γ_1	$\bar{\mu}_0$	$\hat{\chi}^2 \times 10^5$
(i) Const. γ	-25	-0.4	0	-330	5.664	-25	-0.4	0	-340	12.079
(ii) Ref. [3, 22] γ	-30	-0.3	-0.3	-266	6.068	-25	-0.3	-0.3	-285	8.037
(iii) $\phi_{\text{mnn}}(\gamma(\theta))$	-55	-0.4	-0.2	-318	1.976	-55	-0.4	-0.2	-328	3.340
(i) Const. γ	No mean-field enhancement									
		A	γ_0	γ_1	$\bar{\mu}_0$	$\hat{\chi}^2 \times 10^5$	A	γ_0	γ_1	$\bar{\mu}_0$
(i) Const. γ	-30	-0.4	0	-330	5.369	-30	-0.4	0	-341	11.330
(ii) Ref. [3, 22] γ	-35	-0.3	-0.3	-268	6.086	-30	-0.3	-0.3	-286	7.462
(iii) $\phi_{\text{mnn}}(\gamma(\theta))$	-65	-0.4	-0.2	-325	2.310	-65	-0.4	-0.2	-330	3.112